MOEM

Modern Electronic Materials 4(1): 21–29
DOI 10.3897/j.moem.4.1.33273

Research Article

Magnetic and dielectric characteristics of Nd and Nd-Mg substituted strontium hexaferrite

Basharat Want[1], Bilal Hamid Bhat[1]

1 *Solid State Research Lab., Department of Physics, University of Kashmir, Srinagar-19006, India*

Corresponding author: *Basharat Want* (basharatwant@gmail.com)

Received 17 July 2017 ♦ **Accepted** 16 December 2017 ♦ **Published** 1 May 2018

Citation: Want B, Bhat BH (2018) Magnetic and dielectric characteristics of Nd and Nd-Mg substituted strontium hexaferrite. Modern Electronic Materials 4(1): 21–29. https://doi.org/10.3897/j.moem.4.1.33273

Abstract

A systematic investigation on the phase formation, magnetic, dielectric and impedance properties of strontium hexaferrites doped with Nd and Nd-Mg was performed. All ferrite samples were prepared by the citrate-precursor method and characterized with a combination of *X*-ray diffraction, Vibrating sample magnetometer and impedance analyser. XRD analysis confirms the magnetoplumbite structure with space group *p63/mmc* without any secondary phase. The lattice parameter ratio *c/a* lies in the range of 3.92 to 3.94 and shows that the prepared material exhibits M-type hexagonal structure. An increase in coercivity and a decrease in magnetization were observed for all the samples. Large value of coercivity suggests that these materials are useful in longitudinal recording media. Further, it was found that the value of magnetocrystalline anisotropy constant K_1 decreases with the substitution of Nd and Nd-Mg. Measurement of dielectric loss and dielectric constant were performed as a function of temperature and frequency. Dielectric constant and ac conductivity of $Sr_{0.95}Nd_{0.05}Mg_{0.05}Fe_{11.95}O_{19}$ is more as compared to $Sr_{0.95}Nd_{0.05}Fe_{12}O_{19}$ and $SrFe_{12}O_{19}$ for all frequencies. The value of grain boundary resistance (R_{gb}) of $Sr_{0.95}Nd_{0.05}Fe_{12}O_{19}$ is less as compared to $SrFe_{12}O_{19}$ and $Sr_{0.95}Nd_{0.05}Mg_{0.05}Fe_{11.95}O_{19}$ and vice versa trend is observed in the value of capacitance of the grain boundary (C_{gb}) and in the values of relaxation time (τ_{gb}).

Keywords

strontium hexaferrite, magnetization, dielectric behavior

1. Introduction

Since last few decades, the hexaferrite with M-type structure have been the interest of continuous research due to their various remarkable properties [1, 2]. Exhaustive research work on hexaferrites have been instituted for industrial applications such as computer memory chip, high density recording media, transformer, microwave devices, plastic and permanent magnets [3, 4]. Among the hexaferrite, strontium hexaferrite ($SrFe_{12}O_{19}$) is a most versatile and hard magnetic material, which presents unique properties such as magnificent chemical stability, greater microwave magnetic loss, high Curie temperature, high magnetocrystalline anisotropy, high coercivity and saturation magnetization [5, 6]. The structure, magnetic and dielectric properties of strontium hexaferrite plays an important role in making the magnetic, microwave, electronic and microwave devices. However, the properties and physical process of ferrites are dependent on microstructure and chemistry which in turn depend on the preparation technique and conditions employed for fabrication [7, 8]. Strontium hexaferrites have been synthesized by different techniques like hydrothermal process [9], self-propagating high-temperature synthesis [10], the microwa-

ve-assisted calcination route [11], and the citrate precursor [12]. It is well established that method of preparation, sintering temperature, chemical concentration and even particle size can modify dielectric and magnetic properties of ferrites. Thus, investigation of such properties at various chemical compositions, temperature and frequencies may provide reliable information about the nature of various physical processes. The dielectric and electrical properties are important for hexaferrites, not only from the fundamental but from the technological point of view. The dielectric and electric properties of substituted hexaferrites are equally valuable as those of magnetic properties from the technological point of view. Many investigators have shown that intrinsic properties like electrical, magnetic and optical could be enhanced by substituting hexaferrite with bi-, tri- or tetra -valent metal ions like Cr^{3+}, La^{3+}, Nd^{+3}, [13] Co^{2+}-La^{3+}, Ni^{2+}-Zr^{4+} [14, 15]. Assessment of ac electrical conductivity provides complete information as regard the usefulness of the ferrites for different applications. Further, the analyses of ac conductivity can throw light on the behaviour of charge carriers under an ac field, conduction mechanism and their mobility.

Recent studies have shown that an improvement can be obtained in the magnetic properties of rare-earth (RE) substituted hexaferrite. The improved properties can be associated with the increase the magneto crystalline and coercive field with magnetization.

There are some reports on Nd substitution on the properties of hexaferrites, such as, Zhang et al. [16] have reported the effect of Nd-Co substitution on magnetic and microwave absorption properties of $SrFe_{12}O_{19}$.Sharma et al. [17] reported the influence of Nd^{3+} and Sm^{3+} substitution on the magnetic properties of strontium ferrite sintered magnets. Luo J. [18] studied the structure and magnetic properties of Nd doped strontium hexaferrite nanoparticles. Sadiq et al. [19] reported the influence of Nd-Co substitution on structural, electrical and dielectric properties of *X*-type hexagonal nanoferrites. However, due to low solubility of rare earth, the incorporation of rare earth into hexaferrite lattice leads to the formation of secondary phases which can deteriorate the properties of the prepared material [20, 21].

Accounting all the previous studies we have tried to elucidate the role of rare earth element in substituted M-type hexaferrite in enhancing various properties. For this reason Nd and Nd-Mg strontium hexaferrite with single concentration (x = 0.05) was prepared in order to understand how the various properties vary with the substitution of rare earth and if an enhancement with respect to the parent compound.

2. Experimental Details

$SrFe_{12}O_{19}$, $Sr_{0.95}Nd_{0.05}Fe_{12}O_{19}$ and $Sr_{0.95}Nd_{0.05}Mg_{0.05}Fe_{11.95}O_{19}$ nano-particles have been prepared by citrate-precursor method. The following precursors were used: ferric nitrate nona-hydrate, neodymium nitrate hexahydrate, strontium nitrate anhydrous, magnesium nitrate hexa-hydrate, citric acid anhydrous (purity 99.9%, Sigma Aldrich). The synthetic route was the following: Each nitrate, weighed according to the stoichiometry of each composition, and individual dissolution in distilled water was prepared. After one hour of stirring, all the dissolutions of metal salts and citric acid were mixed in a single one at room temperature. Citric acid anhydrous acts as a fuel. The ratio of nitrates and citric acid was taken as 1:1. The pH of the solution was adjusted at 6.5 by using ammonia solution (25%). The obtained solution was heated at 90 °C till a gel solution was obtained. The so obtained gel was heated till combustion, ultimately leaving only loose ashes. These ashes were grinded by a motor pestle arrangement for about 30 min. The whole powder was then heated at 500°C to remove the organic moiety. Finally the powder was calcinated at 950 °C for 3 h.

The structural phase of the synthesised samples were determined by D8 Advance Bruker X-ray diffractometer with CuK_{α} (λ = 1.5406 Å) radiation. The measurement was taken at the rate of 2°/min and the step size was 0.0198. Magnetization measurements, major hysteresis loops, were obtained at room temperature using a vibrating sample magnetometer (MicroSense EZ9 VSM) with maximum field strength of 2T. The dielectric measurements and impedance spectroscopy measurements of the prepared samples were made by using an impedance analyzer (precision component analyzer by Wayne Kerr electronics, UK) as a function of frequency of the applied ac field (20 Hz to 3 MHz) and as a function of temperature. Silver paint was used as a conducting paste and was applied on both sides of the pellets to make them capacitors with the material as dielectric medium.

3. Results and discussion

3.1. Powder X-ray diffraction results

Fig. 1 shows the XRD pattern of the prepared material. The XRD pattern of the prepared material is characterized by diffraction peaks corresponding to $SrFe_{12}O_{19}$ with the magnetoplumbite structure and space group $p63/mmc$ (PDF No. 41#1373) with no secondary phases. XRD patterns show that gradual decrease in the intensity and an associated broadening of the peaks of the oxides. This indicates a continuous fragmentation of the material by the refinement of its particle size to the nanometre range**.** Various lattice parameters are listed in Table 1.From table 1 lattice constant a, c and volume cell agree with the reported literature [22]. A small change in the lattice pa-

Table 1. Various lattice parameters

Composition	a (Å)	c (Å)	c/a	V_{cell} (Å^3)
$SrFe_{12}O_{19}$	5.92	23.23	3.92	705.51
$Sr_{0.95}Nd_{0.05}Fe_{12}O_{19}$	5.90	23.20	3.93	699.85
$Sr_{0.95}Nd_{0.05}Mg_{0.05}Fe_{11.95}O_{19}$	5.89	23.21	3.94	697.30

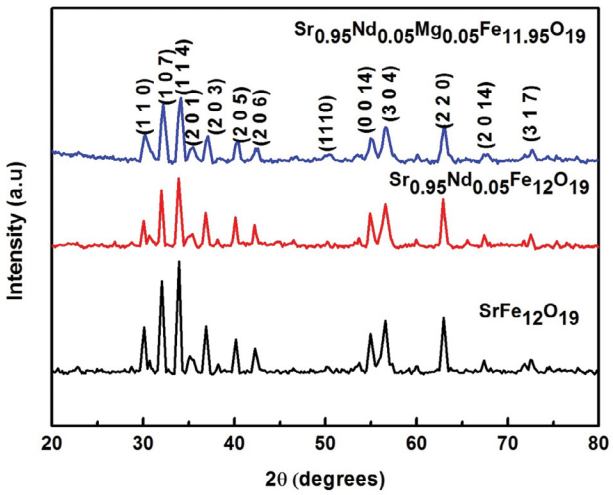

Figure 1. XRD pattern of the $SrFe_{12}O_{19}$ substituted with Nd and Nd-Mg at room temperature, the M-type phase has been indexed according to the calculated spectrum

rameters were observed by the substitution of rare-earth dopants. The lattice parameter ratio c/a lies in the range of 3.92 to 3.94 and shows that the prepared material exhibits M-type hexagonal structure. The similar variation in the lattice parameters have been reported in the Nd doped $SrFe_{12}O_{19}$ nanoparticles [23]. The volume cell was calculated by using the following relation [24].

$$V_{cell} = 0.8666a^2c,$$

where V_{cell} is the volume of the unit cell and 'a' and 'c' are the lattice constant

3.2. Magnetic measurements

Fig. 2 shows magnetic hysteresis loops for all the prepared samples at 300 K. The prepared materials show the behavior of a hard magnetic material with high coercivity and magnetization. It is observed that magnetization of all samples do not saturate even by applying fields up to 2T, and is dominated by domain rotation in the high field region. Therefore, the value of saturation magnetization (M_s) and anisotropy constant K_1, is measured by the Law of Approach to Saturation [25].

$$M = M_S\left(1+\frac{A}{H}+\frac{B}{H^2}\right)+\chi_p H, \quad (1)$$

where H is applied, χ_p is high- field susceptibility, A is the inhomogeneity parameter and the term A/H is associated with the in-homogeneities in the microcrystals. The term B/H^2 is related with the contribution of magnetocrystalline anisotropy. For hexagonal crystals the magnetocrystalline term is given by:

$$B = -\frac{1}{15}H_a^2. \quad (2)$$

The magnetocrystalline anisotropy constant (K_1) is given by the following relation:

$$H_a = \frac{2K_1}{M_S}. \quad (3)$$

where K_1 and H_a are first anisotropy constant and anisotropy field respectively.

A plot of M versus $1/H^2$ in the field range $1T < H < 1.6T$ (Fig. 2) for each sample gave a straight line, suggesting that the contribution from terms A and χ_p are negligible [26, 27]. The saturation magnetization was measured from the intercept of the straight line in conformity with the equation (1). Moreover, the slope of the straight line was used to measure the anisotropy field and the first anisotropy constant in accordance with equations (2) and (3) while as, coercivity is directly estimated from the hysteresis loops. Various magnetic parameters of all samples are listed in table 2. It is evident from the table that saturation magnetization decreases with the substitution of Nd and Nd-Mg [28].The observed results of pure $SrFe_{12}O_{19}$ nanoparticles are consistent with the earlier reports on $SrFe_{12}O_{19}$ [29]. The starting of magnetic behaviour in hexaferrite is due to net magnetic moment of ions with up and down spin in various symmetry sites. Firstly,

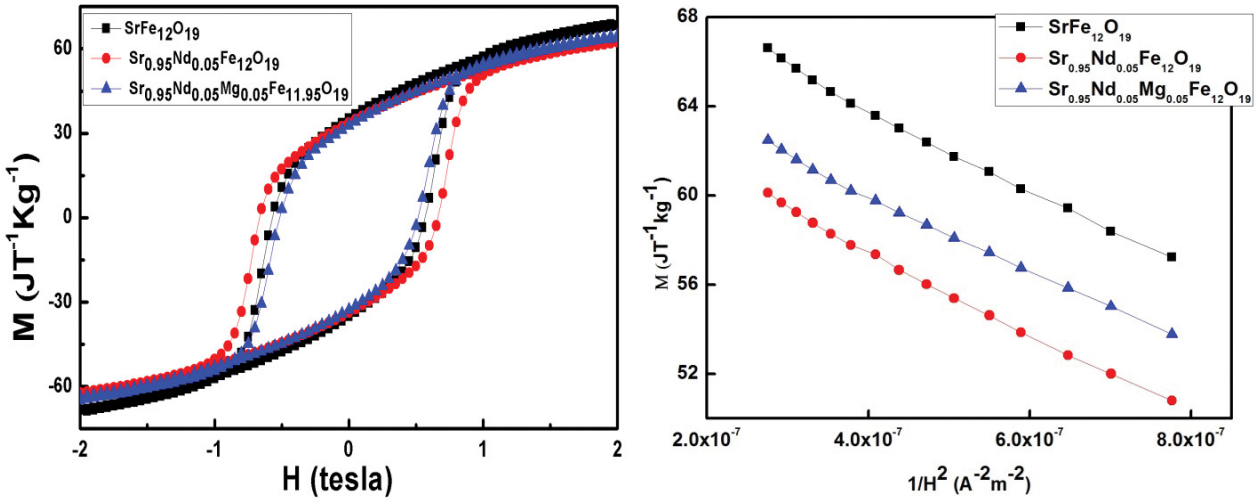

Figure 2. Magnetic hysteresis loops of the $SrFe_{12}O_{19}$ substituted with Nd and Nd-Mg

Table 2. Magnetic parameters of all samples

	M_s (JT^{-1}Kg^{-1})	H_c (kAm^{-1})	H_a (kAm^{-1})	K_1x10^{-2}(J/m^3)
$SrFe_{12}O_{19}$	66.75	453.59	1.421	6.42
$Sr_{0.95}Nd_{0.05}Fe_{12}O_{19}$	62.54	525.21	1.484	6.88
$Sr_{0.95}Nd_{0.05}Mg_{0.05}Fe_{11.95}O_{19}$	60.22	421.76	1.373	5.78

the decrease in saturation magnetization may be assigned to the magnetic dilution due to the substitution of dopants. Secondly, with the substitution of these dopants also weakens the superexchange interaction which may also cause the decrease of the saturation magnetization.

Previous reports [30, 31] have shown that the coercivity depends on magnetocrystalline constant. It is observed that in the present investigation Nd substituted strontium hexaferrite possess large coercivity. The crystalline anisotropy (H_a) varies directly with the substitution of Nd. It can be generalized that the increase of coercivity is attributed to enhancement in crystalline anisotropy field due to substitution of rare earth (Nd). In other word, the substitution of rare earth (Nd) exerts intrinsic effects on the enhancement of coercive field. The value of coercivity of Nd doped hexaferrite is 525.21 kAm^{-1} which is due to strong uniaxial anisotropy along the *c* axis.

As far as the Nd-Mg substituted system is concerned it is observed that there is a decrease in coercivity which is ascribed mainly due to the decrease in crystalline anisotropy field due to substitution of Nd-Mg. The coercivity decrease from 525.21 to 421.76 kAm^{-1}. This result can be ascribed to the decrease in anisotropy field, due to the change of the axis of magnetization from the c-axis to the basal plane [32-34]. It is well-known that the contributions of 2*b* and 4*f*2 sublattice sites in the cyrstalline anisotropy field in the hexaferrite are more than any other sites, while as the contribution from other sites are negligible.

Further, it is reported [35] that if the value of coercivity is more than $M_r/2$, the materials are hard magnets and these are regarded valuable for high frequency applications. If the coercivity is smaller than $M_r/2$, then the materials are semi hard magnets and are useful for information storage technologies [36]. In the present study, the coercivity is more than $M_r/2$, thus the present material are hard magnets and are useful for high frequency applications.

The value of magnetocrystalline anisotropy constant K_1 decreases with the substitution of Nd and Nd-Mg. Further, the magnetocrystalline values are positive and are smaller than the theoretical value for the bulk M-type hexaferrite [37].

3.3. Dielectric studies

(a) Dependence of dielectric behavior on frequency

The dielectric constant in the complex form can be written as:

$$\varepsilon = \varepsilon' - i\varepsilon'' \quad (4)$$

Where ε' is the real part and ε'' is imaginary part designating the stored and dissipated energy respectively. The frequency dependence of real part of dielectric constant of $SrFe_{12}O_{19}$, $Sr_{0.95}Nd_{0.05}Fe_{12}O_{19}$ and $Sr_{0.95}Nd_{0.05}Mg_{0.05}Fe_{11.95}O_{19}$ samples in an ac field ranging from 20 Hz-3MHz is illustrated in Fig. 3. It is observed that the value of dielectric constant decreases continuously with increase in frequency for all the three compositions. The decrease of dielectric constant (ε') and dielectric loss (shown in Fig. 4) with frequency is a general dielectric behavior of ferrites. This type of behavior has been reported by many investigators [38-41] and can be explained on the basis of polarization mechanism. There are four primary mechanism of polarization in materials i.e. electronic, ionic, dipolar and space charge polarization. At low frequencies, all the mechanisms of polarization contribute to the dielectric constant and with the increase in frequency, the contributions from different polarizations starts decreasing. For example, at very high frequencies of the order of 10^{15} Hz, only electronic polarization contributes to the dielectric constant. The constant behavior in dielectric constant at higher frequencies indicates the inadequacy of electric dipoles to follow the variation in frequencies due to alternating applied electric field or it can be interpreted that the electronic exchange between the ferrous and ferric ions i.e, $Fe^{2+} \leftrightarrow Fe^{3+}$ cannot follow the alternating field.

From Fig. 3, it is evident that dielectric constant of $Sr_{0.95}Nd_{0.05}Mg_{0.05}Fe_{11.95}O_{19}$ is higher than $Sr_{0.95}Nd_{0.05}Fe_{12}O_{19}$ and $SrFe_{12}O_{19}$. The possible reason for this behavior can be attributed to the fact that some of iron ions migrate from tetrahedral site to octahedral site due to occupation by Nd and Mg ions. This results in decrease in the resistance of grain there by increasing the probability of electrons reaching the grain boundary which becomes responsible for increase in polarization and hence the dielectric constant. This behavior is in good agreement with impendence spectroscopy data (discussed in section 3.5).

From Fig. 4 it is observed that dielectric loss of $Sr_{0.95}Nd_{0.05}Fe_{12}O_{19}$ is more as compared to $Sr_{0.95}Nd_{0.05}Mg_{0.05}Fe_{11.95}O_{19}$ and $SrFe_{12}O_{19}$. The observed higher values of dielectric loss in the sample $Sr_{0.95}Nd_{0.05}Fe_{12}O_{19}$ is attributed to the formation of vacancies. However, the decrease in loss values of $Sr_{0.95}Nd_{0.05}Mg_{0.05}Fe_{11.95}O_{19}$ can be attributed to the fact that sample with Nd and Mg ions might enhance the conductivity between the grains with the result that the dielectric loss is small in these samples compared with other compound. This is also consistent with the increase in dielectric constant and ac conductivity for $Sr_{0.95}Nd_{0.05}Mg_{0.05}Fe_{12}O_{19}$ compared with other compounds. Dielectric loss is an important part of the total core loss in ferrites [42]. Hence for low core loss, low dielectric losses are desirable.

(b) Dependence of dielectric behavior on temperature

The temperature dependence of the dielectric constant and dielectric loss at 10 kHz for $SrFe_{12}O_{19}$, $Sr_{0.95}Nd_{0.05}Fe_{12}O_{19}$ and $Sr_{0.95}Nd_{0.05}Mg_{0.05}Fe_{11.95}O_{19}$ samples are shown in Fig. 5 and 6. Both dielectric constant and dielectric loss behaves independently at low temperature while at higher temperature it increases with increasing temperature, this behavior at higher temperature is due to generation of extra thermal energy which enhances the mobility of charge carriers hence increases rate of hopping, while as the thermal energy at low temperature does not contribute to mobility of charge carriers. This observed mechanism setup the higher polarization at higher temperature which increases the dielectric constant. It is observed from the plots that dielectric constant and dielectric loss of $Sr_{0.95}Nd_{0.05}Fe_{12}O_{19}$is more as compared to $SrFe_{12}O_{19}$ and $Sr_{0.95}Nd_{0.05}Mg_{0.05}Fe_{11.95}O_{19}$. The reason for this behavior can be attributed to the fact that with temperature there is increase in hopping rate ($Fe^{3+} \leftrightarrow Fe^{2+}$) and also some more vacancies are generated which act as trapping centers. The liberation of charge carriers from these trapping centers needs different energies. This seems to be the main reason for higher value of dielectric constant and loss for the composition $Sr_{0.95}Nd_{0.05}Fe_{12}O_{19}$.

3.4. AC conductivity

The alternating current conductivity (σ_{ac}) is calculated using the following relation:

$$\sigma_{ac} = 2\pi f \varepsilon_o \varepsilon' \tan\delta$$

Where $\varepsilon_o = 8.854 \cdot 10^{-12}$ Fm^{-1} and f is the frequency (in Hz) of the applied electric field. Fig. 7 shows the variation of ac conductivity with frequency at room temperature. A constant behaviour is observed for ac conductivity at lower frequencies [43] and shows a sharp increase at higher

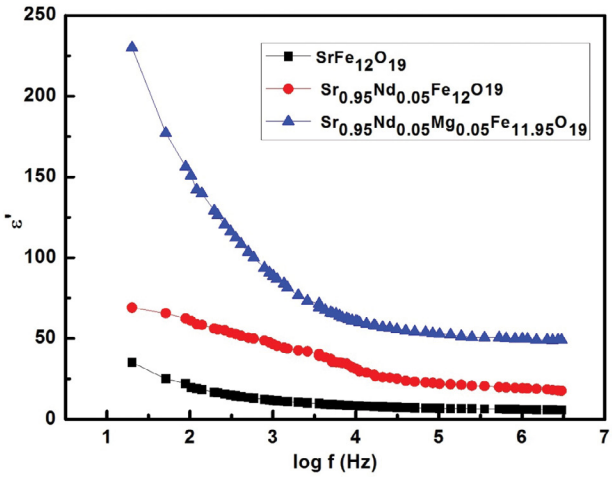

Figure 3. The variation of dielectric constant with frequency of $SrFe_{12}O_{19}$, $Sr_{0.95}Nd_{0.05}Fe_{12}O_{19}$ and $Sr_{0.95}Nd_{0.05}Mg_{0.05}Fe_{11.95}O_{19}$ at room temperature

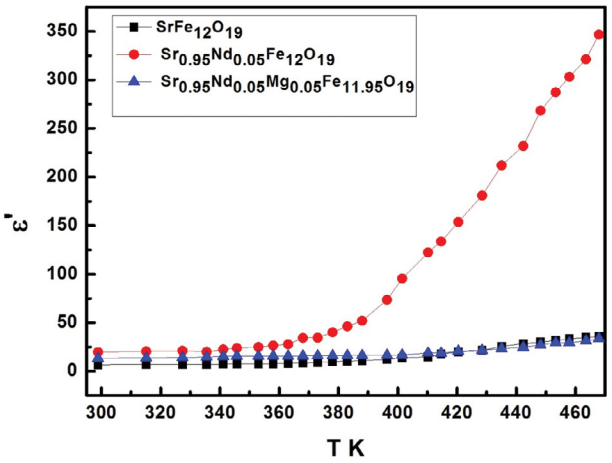

Figure 5. Variation of dielectric constant with temperature at 10 kHz of $SrFe_{12}O_{19}$, $Sr_{0.95}Nd_{0.05}Fe_{12}O_{19}$ and $Sr_{0.95}Nd_{0.05}Mg_{0.05}Fe_{11.95}O_{19}$

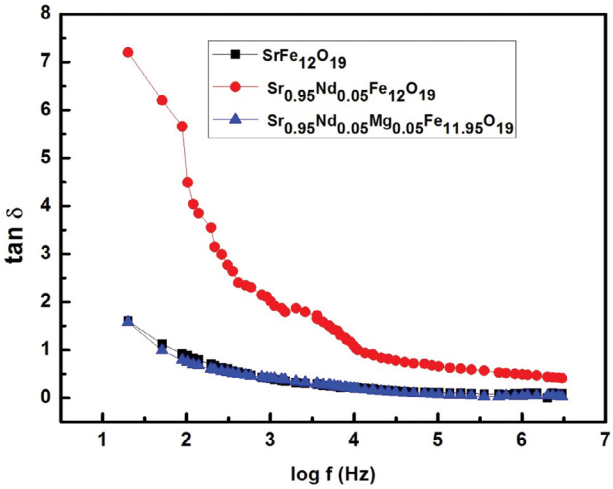

Figure 4. The variation of dielectric loss with frequency of $SrFe_{12}O_{19}$, $Sr_{0.95}Nd_{0.05}Fe_{12}O_{19}$ and $Sr_{0.95}Nd_{0.05}Mg_{0.05}Fe_{11.95}O_{19}$ at room temperature

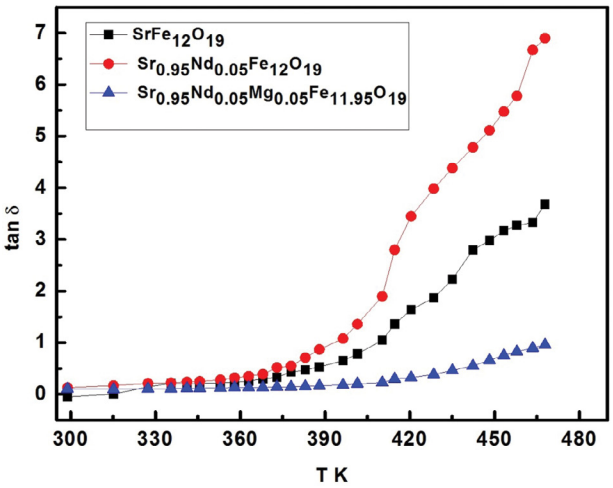

Figure 6. Variation of dielectric loss with temperature at 10 kHz of $SrFe_{12}O_{19}$, $Sr_{0.95}Nd_{0.05}Fe_{12}O_{19}$ and $Sr_{0.95}Nd_{0.05}Mg_{0.05}Fe_{11.95}O_{19}$

frequencies for all compositions. The ac conductivity provides evidence for conduction mechanism whether the charge hopping is between localized states or not. In the present case, the linearity in the plot indicates small polaron type of conduction and is validated in ionic solids [44]. This frequency dependence conduction attributed to small polarons is also reported in the literature [45]. The hopping frequency of the charge carriers seems to depend on the frequency of the applied field and increases in the mobility of charge carriers. At lower frequencies the hopping frequency of electron between ions at the meta interface is less. As the frequency of applied field is increased, the conduction mechanism becomes more active by promoting the hopping of charge carriers between the ions, thereby increasing the hopping frequency. Thus the increase in conductivity at higher frequencies could be due to a reduction in the space charge polarization at higher frequencies [46].

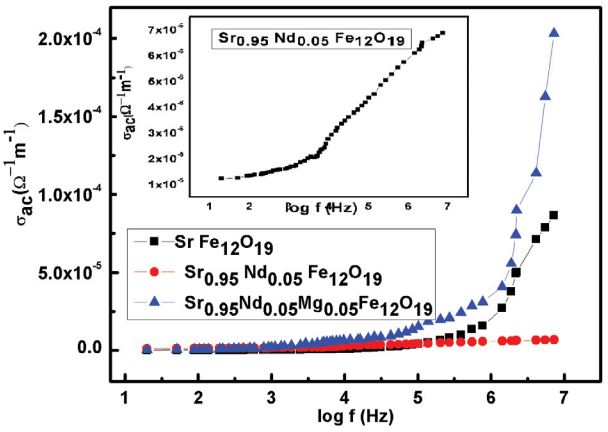

Figure 7. Variation of ac conductivity with frequency of $SrFe_{12}O_{19}$, $Sr_{0.95}Nd_{0.05}Fe_{12}O_{19}$ and $Sr_{0.95}Nd_{0.05}Mg_{0.05}Fe_{11.95}O_{19}$ at room temperature and the inset shows variation of ac conductivity with frequency for $Sr_{0.95}Nd_{0.05}Fe_{12}O_{19}$

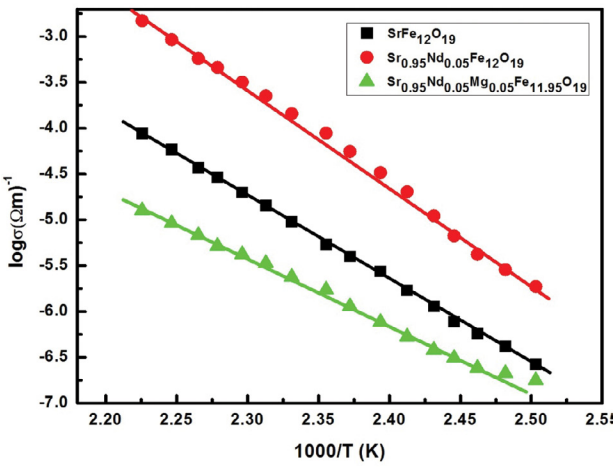

Figure 8. Variation of ac conductivity (at 10 kHz) with reciprocal of temperature of $SrFe_{12}O_{19}$, $Sr_{0.95}Nd_{0.05}Fe_{12}O_{19}$ and $Sr_{0.95}Nd_{0.05}Mg_{0.05}Fe_{11.95}O_{19}$

It is also observed from the plot that ac conductivity of $Sr_{0.95}Nd_{0.05}Mg_{0.05}Fe_{11.95}O_{19}$ is more as compared to $SrFe_{12}O_{19}$ and $Sr_{0.95}Nd_{0.05}Fe_{12}O_{19}$. This behavior can be explained in the same way as that of frequency dependent dielectric constant as there is a direct relation between dielectric constant and dielectric conductivity.

In any case, doping with Nd and Mg ions has resulted in modifications in the dielectric and electrical properties. The investigation thus reveals the possibility of employing doping in controlling the properties of ferrites for specific technological applications.

Fig. 8 shows the variation of ac conductivity (at 10 kHz) with reciprocal of temperature of $SrFe_{12}O_{19}$, $Sr_{0.95}Nd_{0.05}Fe_{12}O_{19}$ and $Sr_{0.95}Nd_{0.05}Mg_{0.05}Fe_{11.95}O_{19}$. The conductivity of these compounds obeys the well known Arrhenius relation [47]:

$$\sigma = \sigma_0 \exp\left(-\frac{E_a}{kT}\right). \quad (5)$$

Where k is Boltzmann constant, Ea is the activation energy required for hopping of charges, T is the absolute temperature and σ_0 specific conductivity. It is observed that the variation of $\ln\sigma_{ac}$ against T^{-1} in the low temperatures range is markedly different from that in the relatively high temperature range. The conductivity is likely to be weakly temperature-dependent in the low temperature range, while it exhibits strong temperature dependence in the high temperature range. This behavior may be attributed to the increase in the drift mobility and hopping frequency of charge carriers with increasing temperature. The charge carriers are considered as localized at the ions or vacant sites and conduction occurs via hopping-type process, which implies a thermally activated electronic mobility.

The calculated values of the activation energy are listed in Table 3. It is observed that activation energy of $Sr_{0.95}Nd_{0.05}Fe_{12}O_{19}$ is more as compared to $SrFe_{12}O_{19}$ and $Sr_{0.95}Nd_{0.05}Mg_{0.05}Fe_{11.95}O_{19}$ This behavior can be explained according to the assumption that the higher activation energy is associated with lower conductivity and dielectric constant [48]. The activation energy of the sample $Sr_{0.95}Nd_{0.05}Mg_{0.05}Fe_{11.95}O_{19}$ has a minimum value, because the energy required for electrons to hop between Fe^{2+} and Fe^{3+} is very small which corresponds to high conductivity and dielectric constant.

3.5. Impedance Spectroscopy

Impedance measurements were carried to get more information about the mechanism of electrical transport as it is

Table 3. The values of activation energy E_a of $SrFe_{12}O_{19}$, $Sr_{0.95}Nd_{0.05}Fe_{12}O_{19}$ and $Sr_{0.95}Nd_{0.05}Mg_{0.05}Fe_{11.95}O_{19}$

Composition	E_a (eV)
$SrFe_{12}O_{19}$	0.873
$Sr_{0.95}Nd_{0.05}Fe_{12}O_{19}$	0.932
$Sr_{0.95}Nd_{0.05}Mg_{0.05}Fe_{11.95}O_{19}$	0.619

a very convenient and powerful experimental technique that enables us to correlate the dielectric properties of a material with its microstructure and the same were carried out for $SrFe_{12}O_{19}$, $Sr_{0.95}Nd_{0.05}Fe_{12}O_{19}$ and $Sr_{0.95}Nd_{0.05}Mg_{0.05}Fe_{11.95}O_{19}$ as a function of frequency (20Hz–3MHz) at room temperature and is shown in Fig. 9.

Depending upon the electrical properties of a material two semi-circles can be obtained from the impedance plot. The first semicircle represents the resistance of grain boundary at low frequency and the second one represents the the resistance of grain or bulk properties at high frequency [49, 50, 51]. The data from impedance measurements can be given in the form

$$Z = Z' + iZ'', \tag{6}$$

here Z' is the real part of impedance that can be related to a pure resistance R, and Z'' is the imaginary part of impedance that can be related to a capacitance C, where $Z'' = 1/j\omega C$. The separation of grain and grain boundary effects can be shown with the help of impedance spectroscopy because each of them has different relaxation time, resulting in separate semi-circles in the complex impedance plot.

The observed semicircles can be explained by equations below.

$$Z' = \frac{R_g}{\left(1 + R_g \omega_g C_g\right)^2} + \frac{R_g}{\left(1 + R_{gb} \omega_{gb} C_{gb}\right)^2}, \tag{7}$$

$$Z'' = \frac{R_g^2}{\left(1 + R_g \omega_g C_g\right)^2} + \frac{R_g^2}{\left(1 + R_{gb} \omega_{gb} C_{gb}\right)^2}, \tag{8}$$

where R_g and C_g represent the resistance and capacitance of the grain and R_{gb} and C_{gb} represent the corresponding terms for grain boundary, while ω_g and ω_{gb} are the frequency at the peaks of the semicircles for grain and grain boundary respectively. The resistances are calculated from the circular arc intercepts on the Z′axis, while the capacitances are derived from the maximum height of the circular arcs. The maximum height in each semicircle is $Z' = -Z''$ therefore by using this condition and using relations above we can calculate the capacitances for grain and grain boundary by using the relations

$$C_g = \frac{1}{R_g \omega_g} \tag{10}$$

$$C_{gb} = \frac{1}{R_{gb} \omega_{gb}} \tag{11}$$

By using the above two relations the relaxation times for grain and grain boundary were calculated as

$$\tau_g = \frac{1}{\omega_g} = R_g C_g \tag{12}$$

$$\tau_{gb} = \frac{1}{\omega_{gb}} = R_{gb} C_{gb} \tag{13}$$

Single semicircle is observed for all compositions which suggest a predominance of the contribution from the grain boundary to the conduction. The various electrical parameters calculated are represented in Table 4. It is observed that the value of grain boundary resistance (R_{gb}) of $Sr_{0.95}Nd_{0.05}Fe_{12}O_{19}$is less as compared to $SrFe_{12}O_{19}$ and$Sr_{0.95}Nd_{0.05}Mg_{0.05}Fe_{11.95}O_{19}$and vice versa trend is observed in the value of capacitance of the grain boundary (C_{gb}) and in the values of relaxation time (τ_{gb}). The decreasing value of resistance in case of $Sr_{0.95}Nd_{0.05}Fe_{12}O_{19}$ signifies that the grain boundary assist in the conduction of charge species. Increase in capacitance signifies conductivity increases, which in turn results an increase in the polarizability of the system. These results are in good agreement with the dielectric measurements.

Table 4. Impedance parameters of $SrFe_{12}O_{19}$, $Sr_{0.95}Nd_{0.05}Fe_{12}O_{19}$ and $Sr_{0.95}Nd_{0.05}Mg_{0.05}Fe_{11.95}O_{19}$ at room temperature

Composition	R_{gb} (M Ω)	C_{gb} (F)	τ_{gb} (s)
$SrFe_{12}O_{19}$	81.91	0.24×10^{-15}	1.96×10^{-6}
$Sr_{0.95}Nd_{0.05}Fe_{12}O_{19}$	7.13	6.6×10^{-1}	4.5×10^{-3}
$Sr_{0.95}Nd_{0.05}Mg_{0.05}Fe_{12}O_{19}$	15.41	5.8×10^{-15}	6.3×10^{-6}

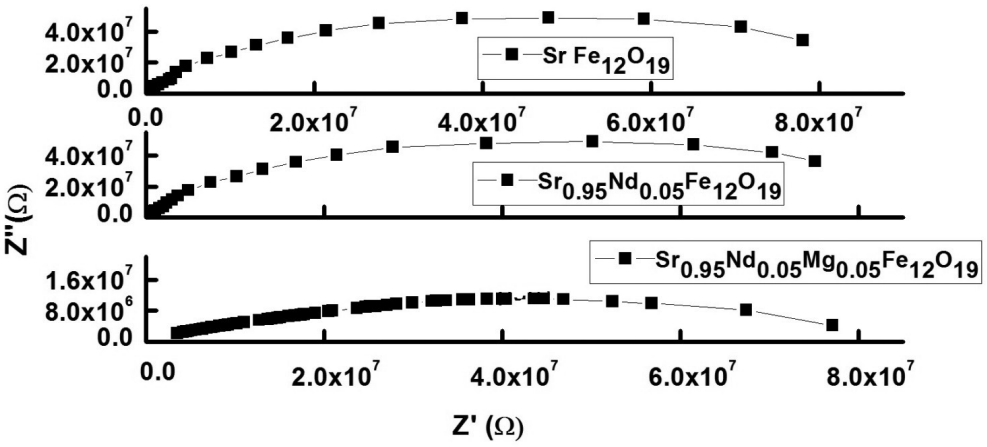

Figure 9. Cole-Cole plot of $SrFe_{12}O_{19}$, $Sr_{0.95}Nd_{0.05}Fe_{12}O_{19}$ and $Sr_{0.95}Nd_{0.05}Mg_{0.05}Fe_{12}O_{19}$ at room temperature

4. Conclusion

The M-type hexaferrites $SrFe_{12}O_{19}$, $Sr_{0.95}Nd_{0.05}Fe_{12}O_{19}$ and $Sr_{0.95}Nd_{0.05}Mg_{0.05}Fe_{11.95}O_{19}$ hexaferrites were successfully synthesized employing citrate-precursor method. Phase formation was confirmed by *X*-ray diffraction. The XRD patterns exhibits that the prepared material were single phase of M-type hexagonal ferrite. The lattice parameter "a" and "c" varied by the substitution of dopants. The incorporation of rare earth cations decreases the saturation magnetization while increase in coercivity from 421 to 525 kAm^{-1}.The magneto crystalline anisotropy constant was found to behave similar to the saturation magnetization with the substitution of dopants, resulting in similar anisotropy fields for all samples. The values of dielectric constant, ac conductivity and activation energy of frequency dependent of $Sr_{0.95}Nd_{0.05}Mg_{0.05}Fe_{11.95}O_{19}$ is more profound that than the $Sr_{0.95}Nd_{0.05}Fe_{12}O_{19}$ and $SrFe_{12}O_{19}$. This may be attributed to the migration of some of iron ions from tetrahedral site to octahedral site due to the occupation of Nd and Mg ions. The value of grain boundary resistance (R_{gb}) of $Sr_{0.95}Nd_{0.05}Fe_{12}O_{19}$is less as compared to $SrFe_{12}O_{19}$ and $Sr_{0.95}Nd_{0.05}Mg_{0.05}Fe_{11.95}O_{19}$and vice versa trend is observed in the value of capacitance of the grain boundary (C_{gb}) and in the values of relaxation time (τ_{gb}). The good magnetic and high dielectric properties of the prepared materials may be useful for high density magnetic recording media and permanent magnets.

References

1. H. Kojimain, Fundamental properties of hexagonal ferrites with magnetoplumbite structure, in: E.P. Wohlfarth (Ed.), Ferromagnetic materials, North Holland, Amsterdam, 1982. 305 p.
2. R.A. McCurrie, Ferromagnetic Materials: Structure and Properties, Academic Press Limited, London (1994) 180–181
3. S.A. Mazen, M.H. Abdallah, R.I. Nakhla, H.M. Zaki, F. Metawe, X-ray analysis and IR absorption spectra of Li–Ge ferrite, Mater. Chem. Phys. 34 (1) (1993) 35–40. https://doi.org/10.1016/0254-0584(93)90116-4
4. J.F. Hochepied, M.P. Pileni, J. Appl. Phys. 87 (2000) 2472. https://doi.org/10.1063/1.372205
5. N. Dishovske, A. Petkov, I. Nedkov, I. Razkazov, Hexaferrite contribution to microwave absorbers characteristics, IEEE Trans. Magn. 30 (1994) 969–971. https://doi.org/10.1109/20.312461
6. S.R. Janasi, M. Emura, F.J.G. Landgraf, D. Rodrigues, The effects of synthesis variables on the magnetic properties of coprecipitated barium ferrite powder, J. Magn. Magn. Mater. 238 (2002) 168–172. https://doi.org/10.1016/S0304-8853(01)00857-5
7. S.J. Lee, C.C.H. Lo, P.N. Matlage, S.H. Song, Y. Melikhov, J.E. Snyder, D.C. Jiles, Magnetic and magnetoelastic properties of Cr-substituted cobalt ferrite, J. Appl. Phys. 102 (2007) 073910. doi: 10.1063/1.2794711J
8. Y. Melikhov, J.E. Snyder, C.C.H. Lo, P.N. Matlage, S.H. Song, K.W. Dennis, D.C. Jiles, The Effect of Cr-Substitution on the Magnetic Anisotropy and Its Temperature Dependence in Cr-Substituted Cobalt Ferrite, IEEE Trans. Magn. 42 (2006) 2861–2863. https://doi.org/10.1109/TMAG.2006.879888
9. M. Jean, V. Nachbaur, J. Bran, J. Le Breton, Synthesis and characterization of $SrFe_{12}O_{19}$ powder obtained by hydrothermal process, J. Alloy Compd. 496 (2010) 306–312. https://doi.org/10.1016/j.jallcom.2010.02.002
10. L. Qiao, L. You, J. Zheng, L. Jiang, J. Sheng, The magnetic properties of strontium hexaferrites with La–Cu substitution prepared by SHS method, J. Magn. Magn. Mater. 318 (2007) 74–78. https://doi.org/10.1016/j.jmmm.2007.04.028
11. Z. Zhou, Z. Wang, X. Wang, X. Wang, J. Zhang, F. Dou, M. Jin, J. Xu, Differences in the structure and magnetic properties of $Sr_{1-x}RE_xFe_{12}O_{19}$ (RE: Pr and Dy) ferrites by microwave-assisted synthesis method, J. Alloys Compd. 610 (2014) 264–270. https://doi.org/10.1016/j.jallcom.2014.04.217
12. X. Liu, W. Zhong, S. Yang, Z. Yu, B. Gu, Y. W. Du, Structure and Magnetic Properties of La^{3+} Substituted Strontium Hexaferrite Particles Prepared by Sol–Gel Method, Phys. Status Solidi A 193 (2002) 314–319. https://doi.org/10.1002/1521-396X(200209)193:2<314::AID-PSSA314>3.0.CO;2-W
13. M.A. Ahmed, N. Okasha, R.M. Kershi, Influence of rare-earth ions on the structure and magnetic properties of barium W-type hexaferrite J. Magn. Magn. Mater. 320 (2008) 1146–1150. https://doi.org/10.1016/j.jmmm.2007.11.014
14. F. Kools, A. Morel, R. Grossinger, J.M. Le Breton, P. Tenaud, La-Co-substituted ferrite magnets, a new class of high-grade ceramic magnets; intrinsic and microstructural aspects, J. Magn. Magn. Mater. 242 (2002) 1270–1276. https://doi.org/10.1016/S0304-8853(01)00988-X
15. M.J. Iqbal, M.N. Ashiq, P.H. Gomez, J.M. Munoz, Magnetic, physical and electrical properties of Zr–Ni-substituted co-precipitated strontium hexaferrite nanoparticles, Scripta.Mater. 57 (2007) 1093–1097. https://doi.org/10.1016/j.scriptamat.2007.08.017
16. Z. Zhang, X. Liu, X.Wang,Y. Wu, R. Li, Effect of Nd–Co substitution on magnetic and microwave absorption properties of $SrFe_{12}O_{19}$ hexaferrites, J. Alloys Compd 525 (2012) 114–119. https://doi.org/10.1016/j.jallcom.2012.02.088
17. P. Sharma, A. Verma, R.K. Sidhu, O.P. Pandey, Influence of Nd^{3+} and Sm^{3+} substitution on the magnetic properties of strontium ferrite sintered magnets. J. Alloys Compd. 361 (2003) 257–264. https://doi.org/10.1016/S0925-8388(03)00390-6
18. J. Lio, Structural and magnetic properties of Nd-doped strontium ferrite nanoparticles, Mater. Lett. 80 (2012) 162–164. https://doi.org/10.1016/j.matlet.2012.04.107
19. I. Sadiq, I. Ali, E.V. Rebrov, S. Naseem, M.N. Ashiq, M.U. Rana, Influence of Nd-Co Substitution on Structural, Electrical, and Dielectric Properties of X-Type Hexagonal Nanoferrites, J. Mater. Eng. Perform. (2013) 622–627.
20. L. Lechevallier, J.M. Le Breton, J.F. Wang, I.R. Harris, Structural analysis of hydrothermally synthesized $Sr_{1-x}Sm_xFe_{12}O_{19}$ hexagonal ferrites J. Magn. Magn. Mater. 269 (2004) 192–196. https://doi.org/10.1016/S0304-8853(03)00591-2

21. H. Mocuta, L. Lechevallier, J.M. Le Breton, J.F. Wang, I.R. Harris,Structural and magnetic properties of hydrothermally synthesised $Sr_{1-x}Nd_xFe_{12}O_{19}$ hexagonal ferrites, J. Alloys Compd. 364 (2004) 48–52. https://doi.org/10.1016/S0925-8388(03)00545-0
22. S. Ounnunkad, Improving magnetic properties of barium hexaferrites by La or Pr substitution, Solid State Commun. 138 (2006) 472–475. https://doi.org/10.1016/j.ssc.2006.03.020
23. Ankush Thakur, R.R. Singh, P.B. Barman, Synthesis and characterizations of Nd^{3+} doped $SrFe_{12}O_{19}$ nanoparticles, Materials Chemistry and Physics 141 (2013) 562–569. https://doi.org/10.1016/j.matchemphys.2013.05.063
24. G.R. Gordani, A. Ghasemi, A. Saidi, Enhanced magnetic properties of substituted Sr-hexaferrite nanoparticles synthesized by co-precipitation method, Ceram. Int. 40 (2014) 4945–4952. https://doi.org/10.1016/j.ceramint.2013.10.096
25. B.D. Cullity, C.D. Graham, Introduction to magnetic materials, Second edition, Wiley, Hoboken, New Jersey, 2009.
26. L. Neel, The law approach: H and a new theory of magnetic hardness, J. Phys. Radium (1948) 184–192. https://doi.org/10.1051/jphysrad:0194800905018400
27. A.T. Aldred, P.H. Froehle, Temperature and field dependence of iron, Int. J. Magn. 2 (1972) 195.
28. T.J. Pérez-Juache, A.L. Guerrero, J.G. Cabal-Velarde, M. Mirabal-García, S.A. Palomares-Sánchez, J.A. Matutes-Aquino, Analysis of the structure and Mössbauer study of the neodymium substitution in the Sr-hexaferrite, Physica B: Physics of Condensed Matter, 503 (2016) 183–188. https://doi.org/10.1016/j.physb.2016.09.026
29. I.A. Auwala, H. Erdemib, H. Sözeric, H. Güngüneşd, A. Baykala, Magnetic and dielectric properties of Bi^{3+} substituted $SrFe_{12}O_{19}$ hexaferrite, J. Magn. Magn. Mater. 412 (2016). https://doi.org/10.1016/j.jmmm.2016.03.066
30. C. Dong, X. Wang, P. Zhou, T. Liu, J. Xie, L. Deng, Microwave magnetic and absorption properties of M-type ferrite $Ba(TiCo)_xFe_{12-2x}O_{19}$ in the Ka band, J. Magn. Magn. Mater. 402 (2013) 80–85. https://doi.org/10.1016/j.jmmm.2014.12.059
31. Reza Shams Alam, MahmoodMoradi, Mohammad Rostami, Hossein Nikmanesh, Razieh Moayedi, Yang Bai, Structural, magnetic and microwave absorption properties of doped Ba-hexaferrite nanoparticles synthesized by co-precipitation method, J. Magn. Magn. Mater. 381 (2015) 1–9.
32. G.R. Gordani, A. Ghasemi, A. Saidi, Enhanced magnetic properties of substituted Sr-hexaferrite nanoparticles synthesized by co-precipitation method, Ceram. Int. 40 (2014) 4945–4952. https://doi.org/10.1016/j.ceramint.2013.10.096
33. S. Kanagesan, S. Jesurani, R.Velmurugan, S. Prabu, T. Kalaivani, Structural and magnetic properties of conventional and microwave treated Ni–Zr doped barium strontium hexaferrite, Mater. Res. Bull. 47 (2012) 188–192. https://doi.org/10.1016/j.materresbull.2011.11.053
34. J. Smit, H.J. Wijn, Ferrites, Philips Technical Library, Eindhoven, The Netherlands (10962), 1962, pp. 316–320.
35. R. Skomki, J.M.D. Coey, Permanent magnetism, CRC Press, 1999. 416 p.
36. I. Ali, M.U. Islam, M.S. Awan, M. Ahmad, Effects of Ga–Cr substitution on structural and magnetic properties of hexaferrite ($BaFe_{12}O_{19}$) synthesized by sol–gel auto-combustion route, J. Alloys Compd. 547 (2013) 118–125. https://doi.org/10.1016/j.jallcom.2012.08.122
37. Y. Huang, Ferromagnetic Materials, Press of University of Electronic Science and Technology of China, Chengdu, 1994.
38. I. Ahmad, G. Murtaza, S. Masood, M. Kanwal, G. Mustafa, M.N. Akhtar, H. Ullah, M. Ahmad, Effects of Pr-contents on the structural, magnetic and high frequency parameters of M-type hexagonal ferrites synthesized by sol–gel method, J. Mater. Sci: Mater. Electron. 27 (6) (2016) 6193–6201. https://doi.org/10.1007/s10854-016-4549-7
39. D. Ravinder, K. Vijay Kumar, Dielectric behaviour of erbium substituted Mn-Zn ferrites, Bull. Mater. Sci. 24 (2001) 505–509. https://doi.org/10.1007/BF02706722
40. R.R. Bhosale, R.S. Barkule, D.R. Shengule, K.M. Jadhav, Synthesis, structural, electrical and dielectric properties of Zn–Zr doped strontium hexaferrite nanoparticles, J. Mater. Sci: Mater. Electron 24 (2013) 3101–3107. https://doi.org/10.1007/s10854-013-1217-z
41. V.V. Somana, V.M. Nanoti, D.K. Kulkarni, Dielectric and magnetic properties of Mg–Ti substituted barium hexaferrite, Ceram. Int., 39 (2013) 5713–5723. https://doi.org/10.1016/j.ceramint.2012.12.089
42. Z. Haijun, L. Zhichao, M. Chengliang, Y. Xi, Z. Liangying, W. Mingzhong, Complex permittivity, permeability, and microwave absorption of Zn- and Ti-substituted barium ferrite by citrate sol–gel process, Mater. Sci. Eng. B 96 (2002) 289-295. https://doi.org/10.1016/S0921-5107(02)00381-1
43. Ashima, Sujata Sanghia, Ashish Agarwal, Reetu, Neetu Ahlawat, Monica, Structure refinement and dielectric relaxation of M-type Ba, Sr, Ba-Sr, and Ba-Pb hexaferrites, J. Appl. Phys. 112 (1) (2012) 014110. https://doi.org/10.1063/1.4734002
44. J. Zhu, K.J. Tseng, C.F. Foo, Effects of multi-segment structure on core losses in MnZn ferrites at high frequencies IEEE Trans. Magn. 36 (2000) 34083410. https://doi.org/10.1109/20.908842
45. K.K. Patankar, S.S. Joshi, B.K. Chougule, Dielectric behaviour in magnetoelectric composites, Phys. Lett. A 346 (2005) 337–341. https://doi.org/10.1016/j.physleta.2005.06.099
46. D. Adler, J. Feinleib, Electrical and Optical Properties of Narrow-Band Materials, Phys. Rev. B 2, 3112 (1970). https://doi.org/10.1103/PhysRevB.2.3112
47. K. Jonscher, Interpretation of non-ideal dielectric plots, J. Mater. Sci. 24 (1989) 372–374. https://doi.org/10.1007/BF00660983
48. M.K. Fayek, S. Mostafa, F. Sayedahmed, S.S. Ata-Allah, M. Kaiser, On the electrical behavior of nickel ferrite-gallates, J. Magn. Magn.Mater. 210 (2000) 189–195. https://doi.org/10.1016/S0304-8853(99)00612-5
49. A.M. A. E. Ata, S.M. Attia, Dielectric dispersion of Y-type hexaferrites at low frequencies, J. Magn. Magn.Mater. 257 (2003) 165–174. https://doi.org/10.1016/S0304-8853(02)00446-8
50. B. Baruwati, R.K. Rana, S.V. Manorama, Further insights in the conductivity behavior of nanocrystalline $NiFe_2O_4$, J. Appl. Phys. 101 (2007) 014302. https://doi.org/10.1063/1.2404772
51. R.K. Kotnala, M.A. Dar, V. Verma, W.A. Siddiqui, Minimizing of power loss in Li–Cd ferrite by nickel substitution for power applications, J. Magn. Magn. Mater. 322 (2010) 3714–3719. https://doi.org/10.1016/j.jmmm.2010.07.033